positive for CC (Fig. 1E). In the motor cortex, severe neuronal loss was also evident and no Betz cells were found (Fig. 1F); immunostaining revealed pTDP-43-positive NCIs mainly in layers II-III and V-VI (Fig. 1G). The histological findings are summarized in Table 1. Diffuse loss of cerebellar Purkinje cells appeared to be attributable to brain ischemia (Table 1).

Table 1 Pathological findings in the present case

Regions	Loss of neuron	pTDP-43-positive NCIs
Cerebral cortex		
Frontal	+++	+++
Motor	+++	+++
Parietal	++	+++
Cingulate	+++	+++
Insular	+++	+++
Entorhinal	++	+++
Hippocampus (DG/Sub)	+/+++	+++/++
Subcortical area		
Amygdala	++	+++
Basal nucleus of Mynert	+	+
Caudate nuclei	+++/+++	+++/+++
Globus pallidus	+	+++
Thalamus (medial/lateral)	++/+++	++/++
Subthalamic nucleus	nd	nd
Midbrain		
Midbrain tectum	+++	+++
Reticular formation	+++	+++
Oculomotor nucleus	+	+
Red nucleus	+	+
Substance nigra	+++	+
Pons		
Locus celreus	++	+
Reticular formation	++	+++
Facial nucleus (motor)	+	++
Vestibular nucleus	+	+
Pontine nucleus	+	++
Superior olivary nucleus	–	–
Medulla oblongata		
Hypoglossal nucleus	+++	–
Dorsal vagal nucleus	+	++
Reticular formation	++	+++
Nucleus ambiguus	nd	nd
Inferior olivary nucleus	+	+
Cerebellum		
Purkinje cell	+++	–
Granule cell	–	–
Dentate nucleus	+	++
Spinal cord		
Anterior horn	+++	+
Intermediate lateral nucleus	++	++
Clarke's nucleus	+++	–
Posterior horn	++	++
Anterior olfactory nucleus	++	++
Dorsal root ganglia	+	+

Loss of neurons: +, mild; ++, moderate; +++, severe. The numbers of pTDP-43-positive neuronal cytoplasmic inclusions (NCIs) were assessed using a semi-quantitative rating scale: –, absent or nearly absent; +, sparse; ++, moderate; +++, numerous. Hippocampus: DG, dentate gyrus (granule cells); Sub, subiculum. nd, not determined.

TDP-43 mutation and *C9ORF72* repeat expansion analyses

Genomic DNA was prepared from a frozen sample of cerebral cortex from the patient, and then examinations for *TDP-43* mutation and *C9ORF72* repeat expansion were carried out as previously described;[8,9] however, neither of these features was found to be present.

Bunina bodies in motor and non-motor neurons

In addition, the occurrence of many eosinophilic NCIs indistinguishable from BBs in the oculomotor nucleus, medullary reticular formation and cerebellar dentate nucleus was a feature of the present patient. Some representative inclusions in the oculomotor nucleus and medullary reticular formation were recycled for electron microscopy, and small tissue blocks from the formalin-fixed cerebellar dentate nucleus were also processed for ordinary electron microscopy. All of the studied NCIs, 2–3 in each region (Fig. 2A–C), were identified as BBs from their characteristic ultrastructural features (Fig. 2D–F). In the medullary reticular formation, the BB-containing neurons were distributed more widely than previously recorded.[6]

We then investigated the presence or absence of CC immunoreactivity in the BBs, as well as the correlation between the occurrence of BBs and that of pTDP-43-positive inclusions. Four-micrometer-thick paraffin sections that contained the bilateral oculomotor nuclei and medullary reticular formation, and unilateral cerebellar dentate nucleus were prepared, and then stained with HE, observed and photographed (Fig. 3A–C,G–I). They were then destained in absolute ethanol and finally immunostained for CC (Fig. 3D–F) or pTDP-43 (Fig. 3J–L). For comparison, the bilateral sacral anterior horns (S1 and S2) and facial motor nuclei were also similarly examined. The degrees of cytoplasmic staining intensity for CC were generally decreased in the LMNs containing BBs (Fig. 1E,3D–F). pTDP-43-positive NCIs appeared as fine to coarse granular (Fig. 3J), linear wisp-like, large irregular (Fig. 3K) or small round-to-oval inclusions (Fig. 3L); the small round-to-oval inclusions were often observed in neurons in the cerebellar dentate nucleus (Fig. 3L). In each region, the ratio of neurons containing CC-positive BBs to the total cell count of neurons containing BBs was calculated in one section. Similarly, the ratio of neurons containing both BBs and pTDP-43-positive inclusions to the total cell count of neurons containing BBs was calculated in one section. The results obtained are shown in Table 2.

DISCUSSION

Based on the distribution and severity of neuron loss and TDP-43 inclusions, the present case was considered to be

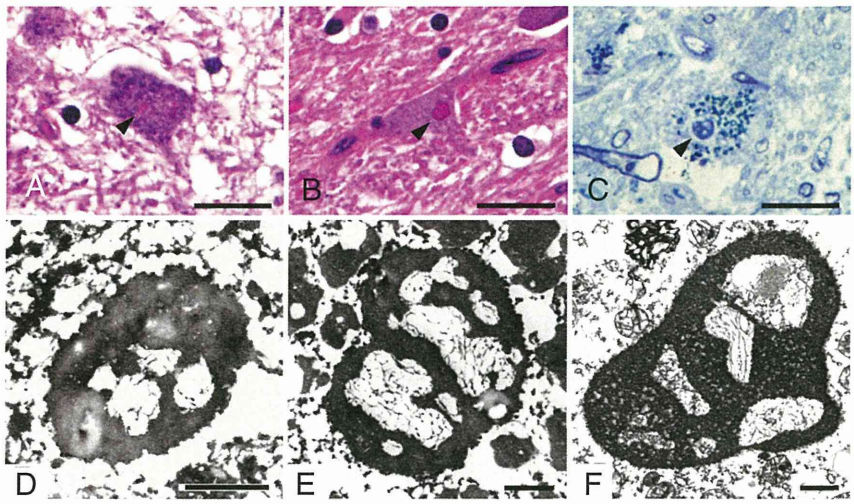

Fig. 2 Ultrastructural profiles of Bunina bodies (BBs) in neurons from the oculomotor nucleus (A), medullary reticular formation (B) and cerebellar dentate nucleus (C). Two paraffin sections stained with HE (A,B) and one Epon section stained with toluidine blue (C). Electron microscopy shows that all the BBs (A–C; arrowheads) have essentially the same ultrastructural profiles, appearing as electron-dense amorphous material with inner clear areas, in which filamentous structures are evident (D–F). In a Bunina body shown in (C), some of the filamentous structures can be identified as neurofilaments, or short fragments of the rough endoplasmic reticulum (F). Scale bars = 20 μm for A–C and 1 μm for D–F.

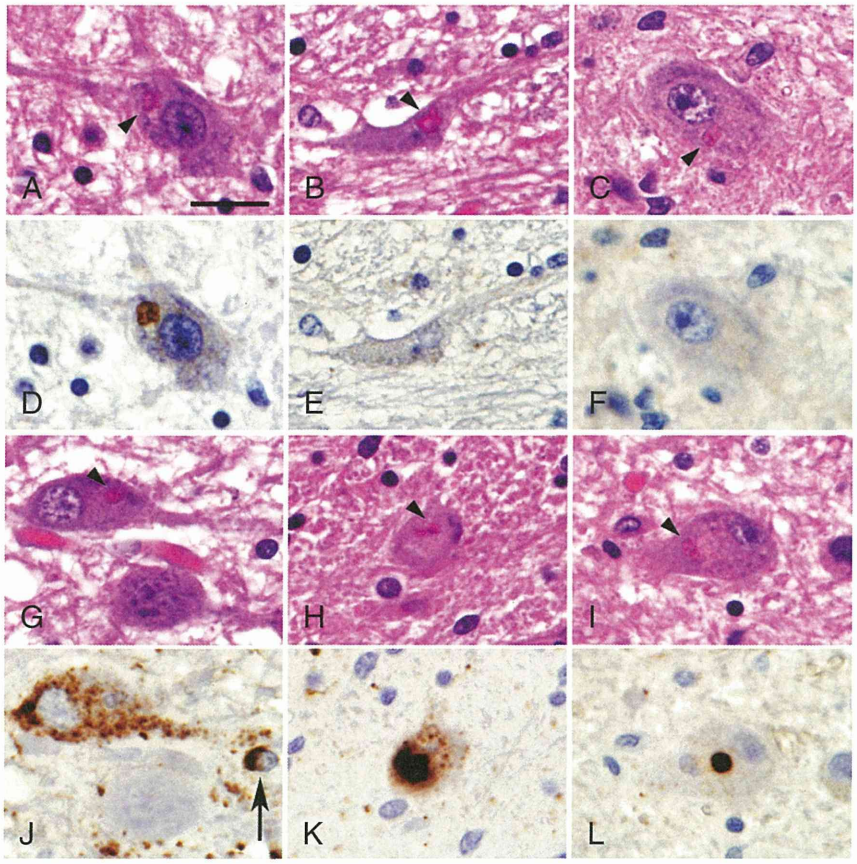

Fig. 3 Immunohistochemical profiles of Bunina bodies (BBs) in neurons from the oculomotor nucleus (A,G), medullary reticular formation (B,H) and cerebellar dentate nucleus (C,I). Sequential staining of the same sections with HE (A–C) and anti-cystatin C (CC) antibody (D–F), as well as with HE (G–I) and anti-phosphorylated trans-activation response DNA protein 43 (pTDP43) antibody (J–L). (A–F) BBs (arrowheads) seen in one lower motor neuron (A) and two non-motor neurons (B,C) are positive (D) and negative (E,F) for CC, respectively. (G–L) In all of the neurons, coexistence of BBs (arrowheads) and pTDP-43-positive neuronal cytoplasmic inclusions (NCIs) is evident; BBs themselves are negative for pTDP-43 (G,J; H,K; I,L). Arrow indicates cytoplasm of a glial cell positive for pTDP-43 (J). Scale bar = 20 μm for (A–L).

an additional example of SALS whose course had been extended by artificial respiratory support, showing widespread multisystem degeneration with TDP-43 pathology (Table 1) (Nishihira *et al.*, Type 2;[10] frontotemporal lobar degeneration – TDP pathology, Type B[11]). We reviewed seven cases in which artificial respiratory support had been used (disease duration, >10 years; Type 1 = 5, Type 2 = 2[10]) and found no NCIs indistinguishable from BBs in the oculomotor nucleus, medullary reticular formation or cerebellar dentate nucleus. In the case (disease duration = $8^2/_3$ years) reported by Nishihira *et al.*,[7] only one BB, which was confirmed by electron microscopy of recycled material, was found in the medullary reticular formation (data not shown). Therefore, the present case, which lacked *TDP-43*

Table 2 Summary of pathological findings for Bunina bodies (BBs)

Region	Ratio (cystatin C)	Ratio (pTDP-43)
Sacral anterior horn	0.88 (7/8)	1.00 (5/5)
Facial motor nucleus	1.00 (8/8)	0.90 (9/10)
Oculomotor nucleus	1.00 (10/10)	1.00 (13/13)
Medullary reticular formation	0.17 (2*/12)†	0.77 (10/13)
Cerebellar dentate nucleus	0.00 (0/36)†	0.33 (12/ /36)††

Ratio (cystatin C): neurons with cystatin C-positive BBs/neurons with BBs; Ratio (pTDP-43): neurons with BBs and pTDP-43-positive inclusions/neurons with BBs. *Regarded as weakly positive. †$P < 0.01$ versus. sacral anterior horn, facial motor nucleus or oculomotor nucleus. ††$P < 0.05$ versus sacral anterior horn, and $P < 0.01$ versus facial motor nucleus, versus oculomotor nucleus or versus medullary reticular formation. Statistical analyses were performed by Ryan's multiple comparison tests using R software (http://www.r-project.org/).

or *C9OLF72* mutation, appeared to be very unusual in terms of the occurrence of BBs even among cases of SALS whose course had been extended by artificial respiratory support.

At present, TDP-43 is widely recognized to be the pathological protein in SALS.[10,12] BBs have been reported to be negative for TDP-43,[12] which was also confirmed in the present study using a monoclonal antibody against pTDP-43. However, the presence of both BBs and TDP-43-positive NCIs has also been shown to be a characteristic feature of ALS with *TDP-43* mutations,[8,12] emphasizing anew the significance of BBs as a specific feature of the cellular pathology of ALS.

Importantly, the present case is the first reported example in which the presence of BBs exhibiting immunoreactivity for CC was a feature of LMNs, but not of non-motor neurons (Table 2). At the ultrastructural level, it is noteworthy that in LMNs, the electron-dense material considered to represent BBs themselves is negative for CC;[5,13] it has been reported that CC immunoreactivity is markedly decreased in the spinal LMNs in SALS, and that the formation of TDP-43 inclusions, but not BBs, may be linked to the CC content of these LMNs.[13] Based on the present findings, we consider that the occurrence of BBs showing CC immunoreactivity is a phenomenon confined almost exclusively to LMNs, and that this must be associated with the particular cellular properties that characterize the LMNs themselves.

The present case is also the first reported to have demonstrated BBs in neurons in the cerebellar dentate nucleus. It has been reported that there is a significant positive correlation between the occurrence of BBs and that of TDP-43 inclusions in spinal and brainstem LMNs.[14,15] This also appears to be the case in the medullary reticular formation (Table 2). However, the ratio (pTDP-43) was significantly lower in the cerebellar dentate nucleus than in other regions (Table 2), indicating that the mechanism responsible for the formation of BBs is distinct from that for TDP-43 inclusions.

Finally, even though the present study involved only a single case and revealed negativity for BBs, as in other similar cases of SALS mentioned above, the results obtained are of considerable interest. In conclusion, the nature and origin of BBs still remain uncertain. When considering why LMNs are generally most vulnerable in ALS, further studies on the formation of BBs in association with the cellular molecular properties of LMNs are needed to elucidate the pathomechanism underlying the disease.

ACKNOWLEDGMENTS

We thank C. Tanda, S. Nigorikawa, J. Takasaki, H. Saito, T. Fujita and S. Egawa for their technical assistance. This work was supported by a Grant-in-Aid, 23240049, for Scientific Research from the Ministry of Education, Culture, Sports, Science and Technology, and a Grant-in-Aid from the Research Committee for CNS Degenerative Diseases, the Ministry of Health, Labour and Welfare, Japan.

REFERENCES

1. Okamoto K, Mizuno Y, Fujita Y. Bunina bodies in amyotrophic lateral sclerosis. *Neuropathology* 2008; **28**: 109–115.
2. Piao YS, Wakabayashi K, Kakita A *et al.* Neuropathology with clinical correlations of sporadic amyotrophic lateral sclerosis: 102 autopsy cases examined between 1962 and 200. *Brain Pathol* 2003; **12**: 10–22.
3. Okamoto K, Hirai S, Amari M, Iizuka T, Watanabe M, Murakami N. Oculomotor nuclear pathology in amyotrophic lateral sclerosis. *Acta Neuropathol* 1993; **85**: 458–462.
4. Okamoto K, Hirai S, Ishiguro K, Kawarabayashi T, Takatama M. Light and electron microscopic and immunohistochemical observations of the Onuf's nucleus of amyotrophic lateral sclerosis. *Acta Neuropathol* 1991; **81**: 610–614.
5. Okamoto K, Hirai S, Amari M, Watanabe M, Sakurai A. Bunina bodies in amyotrophic lateral sclerosis immunostained with rabbit anti-cystatin C serum. *Neurosci Lett* 1993; **162**: 125–128.
6. Nakano I, Iwatsubo T, Hashizume Y, Mizutani T. Bunina bodies in neurons of the medullary reticular formation in amyotrophic lateral sclerosis. *Acta Neuropathol* 1993; **85**: 471–474.
7. Nishihira Y, Tan CF, Toyoshima Y *et al.* Sporadic amyotrophic lateral sclerosis: widespread multisystem degeneration with TDP-43 pathology in a patient after long-term survival on a respirator. *Neuropathology* 2009; **29**: 689–696.

8. Yokoseki A, Shiga A, Tan CF *et al.* TDP-43 mutation in familial amyotrophic lateral sclerosis. *Ann Neurol* 2008; **63**: 538–542.
9. Konno T, Shiga A, Tsujino A *et al.* Japanese amyotrophic lateral sclerosis patients with GGGGCC hexanucleotide repeat expansion in *C9ORF72*. *J Neurol Neurosurg Psychiatry* 2013; **84**: 398–401.
10. Nishihira Y, Tan CF, Onodera O *et al.* Sporadic amyotrophic lateral sclerosis: two pathological patterns shown by analysis of distribution of TDP-43-immunoreactive neuronal and glial cytoplasmic inclusions. *Acta Neuropathol* 2008; **116**: 169–182.
11. Mackenzie IR, Neumann M, Baborie A *et al.* A harmonized classification system for FTLD-TDP pathology. *Acta Neuropathol* 2011; **122**: 111–113.
12. Tan CF, Eguchi H, Tagawa A *et al.* TDP-43 immunoreactivity in neuronal inclusions in familial amyotrophic lateral sclerosis with or without SOD1 gene mutations. *Acta Neuropathol* 2007; **113**: 535–542.
13. Mori F, Tanji K, Miki Y, Wakabayashi K. Decreased cystatin C immunoreactivity in spinal motor neurons and astrocytes in amyotrophic lateral sclerosis. *J Neuropathol Exp Neurol* 2009; **68**: 1200–1206.
14. Mori F, Tanji K, Miki Y, Kakita A, Takahashi H, Wakabayashi K. Relationship between Bunina bodies and TDP-43 inclusions in spinal anterior horn in amyotrophic lateral sclerosis. *Neuropathol Appl Neurobiol* 2010; **36**: 345–352.
15. Mori F, Kakita A, Takahashi H, Wakabayashi K. Co-localization of Bunina bodies and TDP-43 inclusions in lower motor neurons in amyotrophic lateral sclerosis. *Neuropathology* 2013. doi:10.1111/neup.12044

Riku et al. Acta Neuropathologica Communications 2013, 1:12
http://www.actaneurocomms.org/content/1/1/12

ACTA NEUROPATHOLOGICA COMMUNICATIONS

CASE REPORT Open Access

Extensive aggregation of α-synuclein and tau in juvenile-onset neuroaxonal dystrophy: an autopsied individual with a novel mutation in the *PLA2G6* gene-splicing site

Yuichi Riku[1,2], Takeshi Ikeuchi[3], Hiroyo Yoshino[4], Maya Mimuro[5], Kazuo Mano[1], Yoji Goto[1], Nobutaka Hattori[6], Gen Sobue[1] and Mari Yoshida[5*]

Abstract

Background: Infantile neuroaxonal dystrophy (INAD) is a rare autosomal-recessive neurodegenerative disorder. Patients with INAD usually show neurological symptoms with infant onset and die in childhood. Recently, it was reported that mutations in the *PLA2G6* gene cause INAD, but neuropathological analysis of genetically confirmed individuals with neuroaxonal dystrophy has been limited.

Results: Here, we report a Japanese individual with neuroaxonal dystrophy associated with compound heterozygous mutations in the *PLA2G6* gene. A novel splice-site mutation resulting in skipping and missense mutations (p.R538C) in exon 9 was identified in the patient. This patient initially presented with cerebellar ataxia at the age of 3 years, which was followed by symptoms of mental retardation, extrapyramidal signs, and epileptic seizure. The patient survived until 20 years of age. Neuropathological findings were characterized by numerous axonal spheroids, brain iron deposition, cerebellar neuronal loss, phosphorylated alpha-synuclein-positive Lewy bodies (LBs), and phosphorylated-tau-positive neurofibrillary tangles. In particular, LB pathology exhibited a unique distribution with extremely severe cortical involvement.

Conclusions: Our results support a genetic clinical view that compound heterozygous mutations with potential residual protein function are associated with a relatively mild phenotype. Moreover, the severe LB pathology suggests that dysfunction of the *PLA2G6* gene primarily contributes to LB formation.

Keywords: α-synuclein, Infantile neuroaxonal dystrophy, Atypical neuroaxonal dystrophy, PLA2G6 gene, Tau

Background

Neurodegeneration with brain iron accumulation (NBIA) describes a group of progressive neurodegenerative disorders that are pathologically characterized by the presence of axonal spheroids and iron deposition in the brain [1-3]. These neurodegenerative diseases consist of a clinically and genetically heterogeneous group of disorders, including pantothenate kinase-associated neurodegeneration (PKAN, formerly known as Hallervorden-Spatz disease), infantile neuroaxonal dystrophy (INAD), and an unknown gene mutation-linked idiopathic neuroaxonal dystrophy [1,2,4]. PKAN is caused by mutations in the pantothenate kinase 2 (*PANK2*) gene, which accounts for the majority of NBIA patients [2]. Recently, it was reported that mutations in the phospholipase A2 group VI (*PLA2G6*) gene cause INAD [5], which is a rare autosomal-recessive neurodegenerative disorder. Patients with INAD usually present with psychomotor regression, truncal hypotonia, progressive ataxia, extrapyramidal symptoms, fast waves on an electroencephalogram, and neuro-ophthalmological abnormalities (e.g., optic atrophy, nystagmus, and strabismus) with infant onset and die in childhood [1,4,6]. However, in rare cases, patients with NAD caused by *PLA2G6* mutations present with heterogeneous neurological manifestations with onset past infanthood and survive until

* Correspondence: myoshida@aichi-med-u.ac.jp
[5]Institute for Medical Science of Aging, Aichi Medical University, Aichi, Japan
Full list of author information is available at the end of the article

adulthood with a slower disease progression [1,7,8]. In addition, mutations of the *PLA2G6* gene cause early onset dystonia-parkinsonism (PARK-14), which is clinically distinguished from NAD by good L-dopa responsiveness, L-dopa–induced dyskinesia, and dementia. These characteristics have been typically observed in patients with an older age of onset and with a longer disease duration compared to NAD, with no evidence of cerebellar symptoms [9]. Thus, these clinical phenotypes are collectively termed as *PLA2G6*-associated neurodegeneration [9].

We report a Japanese individual with neuroaxonal dystrophy that was associated with a novel compound heterozygous mutation in a splicing site of the *PLA2G6* gene. The clinical phenotype of this patient was atypical for INAD, occurred during late disease onset, and prolonged the disease course. Histopathological data revealed the presence of neuroaxonal spheroids, brain iron depositions, and cerebellar degeneration. Moreover, numerous Lewy bodies (LBs) and neurofibrillary tangles (NFTs), which are pathological hallmarks of Parkinson's disease (PD) and Alzheimer's disease (AD), respectively, were observed. Until recently, neuropathological analysis of genetically confirmed neuroaxonal dystrophy has been strongly limited due to a small number of patients [1,8]. In this study, we describe the clinicopathological characteristics of the patient and discuss the neuropathological implication of LBs and NFTs compared with PD and AD.

Case presentation

Clinical history

The patient was a Japanese man who died at 20 years of age. He exhibited normal development until the age of 3 years, at which time his parents noted his slurred speech and unstable gait. There was no evidence of a consanguineous marriage in any of his relatives. His grand-aunt had been diagnosed with "parkinsonism", and she died at the age of 60; however, her clinical diagnosis was uncertain. At the age of six, the patient was referred to our hospital due to a progressive gait disturbance and dysarthria. A neurological examination revealed cerebellar ataxia, bradykinesia, mental retardation, and hyperreflexia in the lower limbs without pathological reflexes. Truncal hypotonia and abnormalities in eye movement were not observed. Cerebral computed tomography (CT) showed severe cerebellar atrophy. The patient was clinically diagnosed with juvenile spinocerebellar degeneration, and taltirelin was administered for his ataxia; however, it did not have an effect. At the age of 12, cerebral magnetic resonance imaging (MRI) revealed severe atrophy of the cerebellum and mild atrophy of the frontal lobes (Figure 1a-c). The patient gradually became bedridden until the age of 15 and started experiencing repetitive generalized seizures. He was mainly treated with sodium valproate and phenobarbital. At the age of 18, he was re-admitted to our hospital, although he was nearly bedridden and could barely sit in a wheelchair at that time. Neurological examination revealed severe dystonia and rigidity in his limbs and neck, a masked face, and severe cerebellar ataxia. His tendon reflexes showed hyperreflexia in the upper limbs and were abolished in his lower limbs. Moreover, his plantar responses were flexor. CT and MRI (Figure 1d-f) revealed severe cerebellar and fronto-temporal lobe atrophy. The cerebral atrophy was more progressive compared to the atrophy observed when he was 12 years old. By T2-weighted imaging (T2WI), the bilateral globus pallidus (GP) and putamen exhibited low signal intensity. Tc99m-ECD-single-photon emission computed tomography revealed hypoperfusion in the fronto-temporal lobes and cerebellum (Figure 1g). An electroencephalogram showed multifocal spikes and theta waves in the right hemisphere in the absence of fast waves. The results of the nerve conduction study on the four limbs were normal. After discharge, a higher dose of valproate reduced the frequency of the patient's seizures; however, his rigidity and dystonia showed no response to L-DOPA treatment. The patient died of aspiration pneumonia.

Materials and methods

Neuropathological analysis

The postmortem interval was 5 hours. The brain and spinal cord were fixed in 20% neutral formalin. Samples obtained from the main representative regions of the brain and spinal cord were embedded in paraffin, sectioned into 4.5-μm-thick slides, and stained with hematoxylin and eosin (H&E), Klüver-Barrera staining, Prussian blue methods, and Gallyas-Braak (GB) staining. Immunohistochemical studies were performed on 4.5-μm-thick sections using an ENVISION kit (Dako) with diaminobenzidine (DAB; Wako, Osaka, Japan) as a chromogen. The primary antibodies used were anti-phosphorylated alpha-synuclein (p-α-synuclein) (pSyn#64, monoclonal mouse, 1:1000; Wako Pure Chemical Industries, Osaka, Japan), anti-ubiquitin (polyclonal rabbit, 1:2000; Dako), anti-amyloid-beta peptide (6F/3D, monoclonal mouse, 1:200; Dako), phosphorylated tau (p-tau) (AT8, monoclonal mouse, 1:2000; Innogenetics, Zwijndrecht, Belgium), anti- TDP-43 (TARDBP, polyclonal rabbit, 1:2500; ProteinTech, IL, USA), and anti-phosphorylated neurofilament (p-NF) (2F11, monoclonal mouse, 1:600; Dako). For double-immunofluorescence labeling, brain tissues obtained from the amygdala, oculomotor nucleus, and substantia nigra were sectioned into 4.5-μm-thick slides. The primary antibodies were anti-p-α-synuclein antibody and AT8 antibody. The secondary antibodies were goat anti-mouse IgG coupled with either

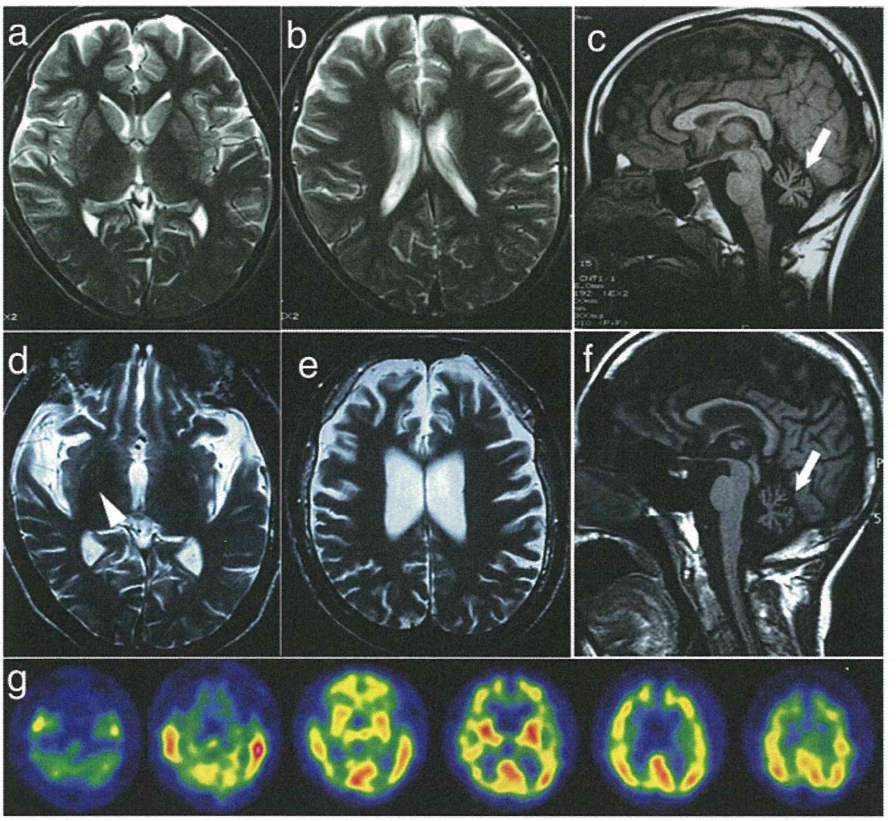

Figure 1 Magnetic resonance imaging (MRI) and Tc99m-ECD-single-photon emission computed tomography (SPECT) of the patient. **a-c** MRI at age 12. There was mild atrophy of the frontal cortex and slightly low intensity in the globus pallidus on T2-weighted images (T2WI) (**a, b**). The saggital section of the T1WI exhibited cerebellar atrophy (arrow) (**c**). **d-f** MRI at age 18. Low signal intensity in the globus pallidus (arrowhead) and atrophy of the temporal lobes was clear on the T2WI (**d**). The frontal lobes showed severe atrophy (**e**). The saggital section of the T1WI exhibited severe cerebellar atrophy (arrow) and thinness of the corpus callosum (**f**). An ECD-SPECT, at age 18, revealed hypoperfusion of the frontotemporal lobes and cerebellum (**g**).

Alexa Fluor 568 (1:300, emission peak 603 nm, Molecular Probes, OR, USA) or Alexa Fluor 488 (1:300, emission peak 517 nm, Molecular Probes). The slides were examined via confocal microscopy at × 200 and × 400 magnification using a Zeiss LSM 710 laser scanning confocal microscope.

For electron microscopy, sections from the cingulate gyrus were fixed in 4% glutaraldehyde. The sections were washed in phosphate buffer, postfixed with osmium tetroxide, dehydrated in a graded series of ethanol, and embedded in Epon. Ultrathin sections were stained with uranyl acetate and lead citrate.

Western blotting analysis of α-synuclein

Proteins expressed in the amygdala and parahippocampal gyrus of the autopsied patient and three control subjects were extracted as previously described [10,11]. Briefly, we fractionated the samples by resolubilization in increasingly stringent buffers (Tris-buffered saline, 1% Triton X-100, 1% sarcosyl, 8 M urea) as previously described. Equal amounts of supernatant protein were subjected to sodium dodecyl sulfate-polyacrylamide gel electrophoresis and immunoblotting. The mouse monoclonal antibody LB509 (Zymed Laboratories, South San Francisco, California) was used to detect α-synuclein. The monoclonal antibody pSyn#64 (Wako, Japan) specifically recognizes phosphorylated α-synuclein at serine 129 [12].

Genetic analysis

Genomic DNA was extracted from the frozen liver tissue of the patient using a standard procedure. Mutational analysis was performed using sequences of both strands of all of the PCR-amplified coding exons and the flanking intronic sequences of *PLA2G6, PANK-2, SNCA, parkin, PINK-1*, and *DJ-1*. Expansion of the CAG repeats of the SCA1, SCA3, DRPLA, and Huntington's disease genes was also examined. Genetic analysis of *PLA2G6* was also performed in the patient's parents. Total RNA was isolated from frozen brain tissue of the patient, and cDNA was synthesized using a High-Capacity cDNA

Reverse Transcription kit (Applied Biosystems). RT-PCR was performed using primer pairs to amplify the coding regions of the *PLA2G6* gene spanning exons 8–13 (5′-caacgtggagatgatcaagg-3′ and 5-gtcagcatcaccttgggttt-3′) and exons 9–13 (5′-ggaaggcgatcttgactctg-3′ and 5′-gtcagcatcaccttgggttt-3′). The institutional review board approved this study.

Results

Neuropathological findings

The patient's height was 150 cm, and his body weight was 39 kg. The brain weighed 890 g before fixation. Grossly, the cerebral hemispheres showed severe atrophy, particularly in the fronto-temporal cortex. In the brain sections, the most striking pathological finding was a light yellow-brown discoloration of the substantia nigra (SN), periaqueductal gray matter, putamen, caudate head, and GP (Figure 2a,b). The cerebellum was greatly reduced in size; its overall convolution pattern was retained, but the individual folia were shrunken.

Histopathologically, severe neuronal loss and gliosis were observed in the cerebral cortex, brainstem gray matter, and cerebellar cortex. In the cerebrum, neuronal loss was marked in the cingulate gyrus, fronto-temporal cortex, insular cortex, amygdala, and hippocampus. In the brain stem, neurons in the SN were markedly depleted, and the remaining neurons had low melanin content. The locus ceruleus (LC) showed moderate neuronal loss, but the neurons in the dorsal motor nucleus of the vagus were relatively spared. The cerebellar cortex showed severe neuronal loss (Figure 2c,d), particularly in the granule cell (gc) layer, and the parallel

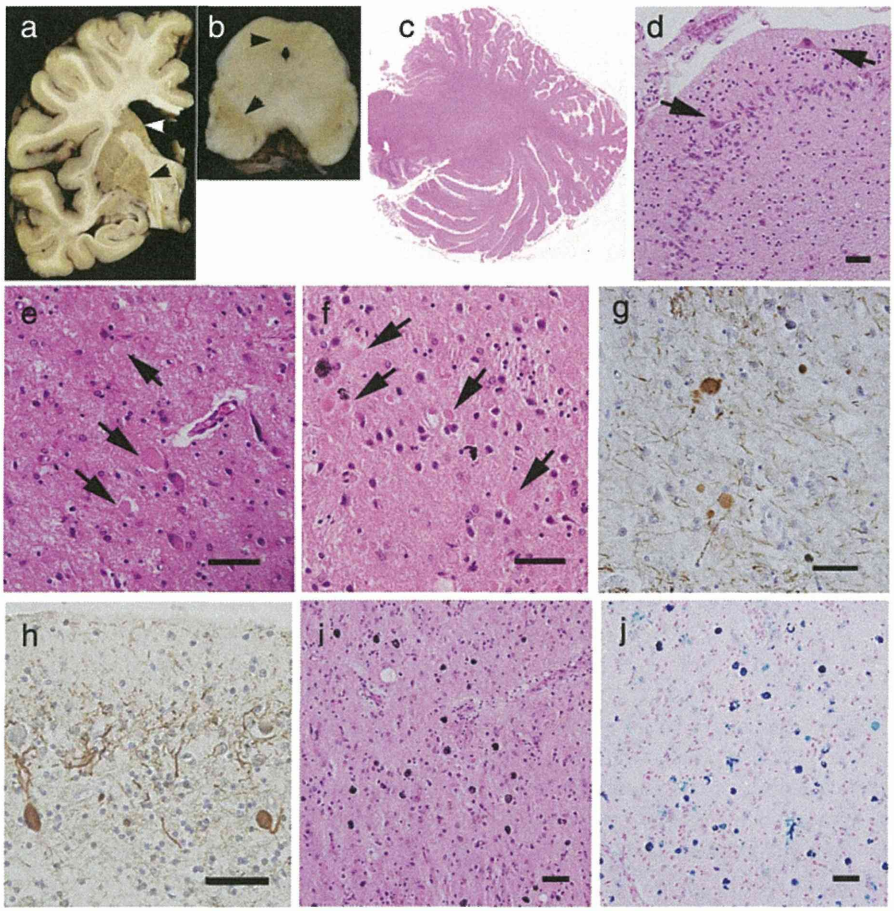

Figure 2 The macroscopic and microscopic findings in the patient. a, b The globus pallidus, putamen, caudate, substantia nigra, and periaqueductal gray matter demonstrated yellow-brown discoloration (arrowheads). **c** Grossly, the cerebellar cortex showed severe atrophy, and the granule cell layer was not visible. **d** The cerebellar granule cells were markedly depleted, and ectopic Purkinje cells (Pcs) were found (arrows). **e** The cingulate gyrus showed gliosis and numerous axonal spheroids (arrows). **f, g** The putamen also contained numerous axonal spheroids that were labeled by anti-phosphorylated neurofilament antibody. **h** In the cerebellum, anti-phosphorylated neurofilament immunostaining revealed dystrophic axons of the Pcs and highly reduced parallel fibers. **i** Many iron-positive granules were observed in the putaminal neuropil. **j** These granules were evident after Prussian blue staining. Bar = 50 μm. Hematoxylin and eosin staining (**c-f, i**), phosphorylated neurofilament immunohistochemistry (**g, h**), and Prussian-blue staining (**j**).

fibers in the molecular layer were strongly reduced (Figure 2c,d,h). Purkinje cells (Pcs) were severely depleted and often ectopically scattered at random in the molecular layer (Figure 2d). The spinal cord exhibited myelin pallor of the gracile fasciculus with gliosis.

In addition, we observed axonal spheroids throughout the central nervous system (CNS), particularly in the cerebral cortex, putamen (Figure 2e-g), caudate nucleus, nucleus accumbens, hypothalamus, SN, gracile nucleus, and spinal cord. The cerebellum contained numerous dystrophic axons called 'torpedoes' in the Pc and gc layers (Figure 2h). The diameters of the spheroids ranged from 10 to 20 μm, but the spinal cord contained larger-sized spheroids of 40–70 μm in diameter. Various spheroids were immunoreactive against anti-p-NF (Figure 2g,h) and anti-ubiquitin antibodies. We found no spheroids in the sympathetic ganglia, dorsal root ganglia, spinal roots, peripheral nerve fibers in the skin, or the enteric plexus. Brown-pigmented, Prussian blue-positive iron granules were scattered around the vessels and throughout the neuropil in the putamen, internal segment of the GP, caudate nucleus, thalamus, pars compacta of the SN, and periaqueductal gray matter (Figures 2i,j, 4c).

Furthermore, severe LB pathology was observed throughout the brain (Figures 3a-f, 4a). In immunohistochemistry, anti-p-α-synuclein (Figure 3c-f), anti-p-NF, and anti-ubiquitin antibodies strongly labeled LBs. Immunohistochemistry using anti-p-α-synuclein antibody also revealed numerous dilated and sausage-like dystrophic neurites in the neuropil, which have been referred to as Lewy neurites (LNs) (Figure 3d,e). In the

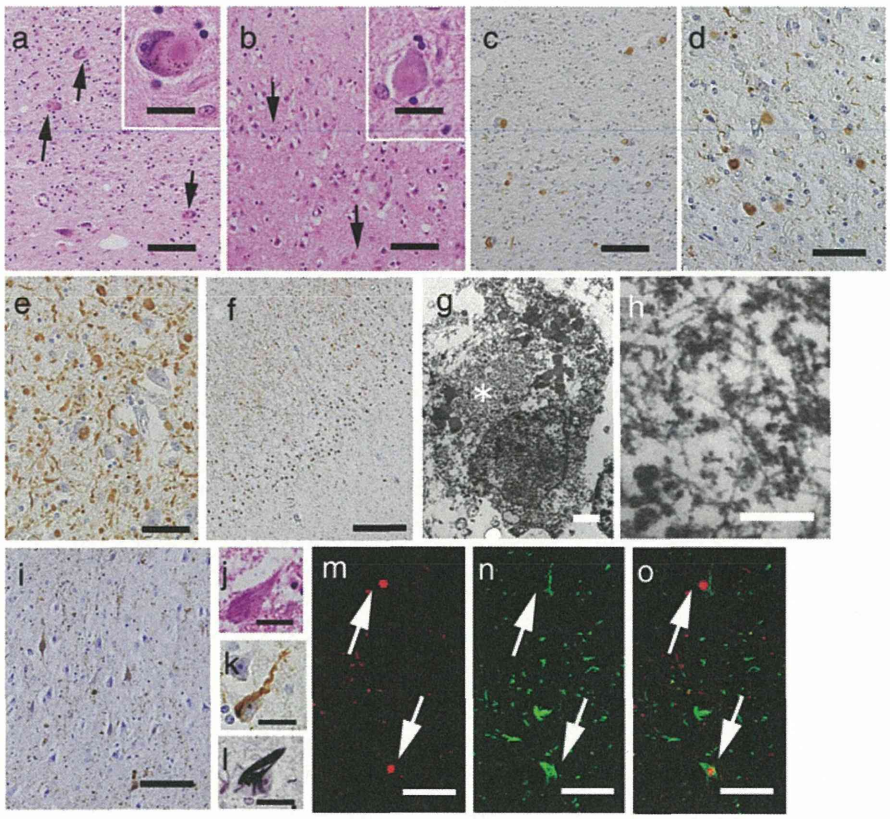

Figure 3 Lewy body (LB) and neurofibrillary tangle (NFT) pathology of the patient. a and inset The substantia nigra contained "brainstem-type" LBs with core and halo (arrows) structures. **b and inset** In the cingulate gyrus, the neuropil showed spongy changes in the deep layer, and there were "cortical-type" LBs without core and halo structures (arrows). **c and d** Anti-phosphorylated alpha-synuclein (p-α-synuclein) immunohistochemistry showed abundant LBs in the substantia nigra (**c**) and cingulate gyrus (**d**). **e and f** In the hypothalamus (**e**) and Ammon' s horn (**f**), p-α-synuclein-positive LBs and LNs were strikingly abundant. **g and h** Electron microscopy of a neuron in the cingulate gyrus showed cortical LBs in a cortical neuron (asterisk), which consisted of granular and filamentous structures. The filaments were arranged at random without a clear central zone density. **i - l** The pyramidal neuron in the hippocampal cortex contained abundant NFTs and threads that were positive for AT-8 antibody using the Gallyas-Braak method. **m-o** Confocal microscopy of the amygdala revealed immunoreactivity against p-α-synuclein (**m**, red), which often co-labeled with AT8 (**n**, green) in the same neurons (**o**, merged). Bar (**a**), (**b**), (**c**), and (**i**) = 100 μm; (**d**), (**e**), (**m**), (**n**), and (**o**) = 50 μm; (**f**) = 250 μm; (**g**) = 2 μm; (**h**) = 0.2 μm; (**a-inset**), (**b-inset**), (**j**), (**k**), and (**l**) = 20 μm. Hematoxylin and eosin staining (**a, b, j**), p-α-synuclein immunohistochemistry (**c-f**), AT8 immunohistochemistry (**i, k**), and Gallyas-Braak staining (**l**).

cerebral cortices, numerous cortical-type LBs, which lacked core and halo structures, and LNs were diffusely found (Figure 3b,e) with striking spongiform alterations (Figure 3b). The distribution and density of LBs and LNs exceeded what has been observed in advanced PD or DLB in the neocortical stage [13,14]. They were most abundant in the cingulate gyrus, amygdala, anterior hippocampus, CA2 region of the posterior hippocampus, and hypothalamus. LBs with a core and halo (brainstem-type LBs) were observed predominantly in the nucleus basalis of Meynert, SN, oculomotor nucleus, and LC (Figure 3a,c). In the cerebellum, neuronal cytoplasm and neurites of the dentate nucleus rarely contained p-α-synuclein-positive structures. In contrast, the olfactory bulbs and dorsal motor nucleus of the vagus contained only mild LB pathology. There were no p-α-synuclein-positive structures in the peripheral sympathetic ganglia, dorsal root ganglia, cardiac sympathetic nerve fibers, or nerve plexuses in the gastroenteric organs. Numerous p-tau-positive NFTs were also found predominantly in the limbic system (Figures 3i-l, 4b). The abundance of NFTs corresponded to AD in Braak stage IV [15], however, Aβ-positive neuritic plaques and amyloid deposits were absent. Additionally, TDP-43-positive inclusions were absent in this patient.

Using double-immunofluorescence labeling in the amygdala, p-tau-positive NFTs and p-α-synuclein-positive cortical LBs often co-labeled in the same neuron (Figure 3m-o). In contrast, neurons in the midbrain did not show co-labeling of LBs and NFTs (data not shown).

On electron microscopy, LBs from the cingulate gyrus consisted of closely packed 6- to 10-nm-thick granular and filamentous structures. The filaments were arranged at random without a clear central zone density. These findings were similar those observed in cortical-type LBs in the DLB [16] (Figure 3g,h).

Western blotting analysis of α-synuclein

To biochemically characterize the accumulation of α-synuclein, we sequentially extracted proteins from the amygdala and parahippocampal gyrus of the autopsied male subject using buffers with increasing capacities to solubilize proteins. In the control sample, immunoblotting analysis using anti-α-synuclein LB509 showed an approximately 15-kDa band corresponding to monomeric α-synuclein in Tris–HCl- and Triton X-100-soluble fractions (Figure 5a). In contrast, an ~15-kDa α-synuclein band was predominantly visualized in sarkosyl-insoluble urea-soluble fractions in the brain (Figure 5a). In addition to the ~15-kDa band, an ~30-kDa band corresponding to α-synuclein dimers was observed in the insoluble fractions extracted from the patient's brain samples. Importantly, the ~15- and ~30-kDa bands found in the urea-extracted fractions were reactive to anti-pSyn#64 antibody (Figure 5b), indicating that the accumulated α-synuclein in the patient brain

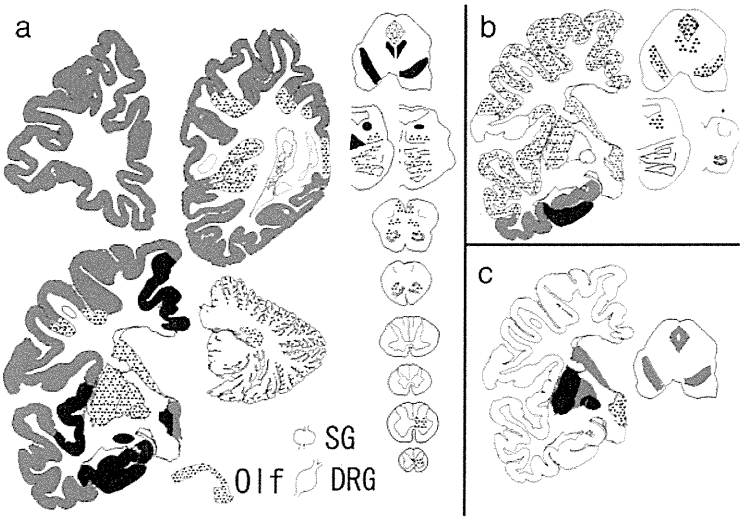

Figure 4 Schema of the distribution of Lewy bodies (LBs), neurofibrillary tangles (NFTs), and iron deposition in the patient. a LBs were diffusely spread in the cerebral cortices and were most abundant in the limbic system, hypothalamus, nucleus basalis of Meynert, substantia nigra (SN), and locus ceruleus. The olfactory bulbs and dorsal motor nucleus of the vagus contained only mild LB pathology. There were no p-α-synuclein-positive structures in the peripheral sympathetic ganglia and dorsal root ganglia. **b** NFTs were predominantly observed in the limbic system, which corresponded to Alzheimer's disease in Braak stage IV. **c** Iron-positive granules were found in the putamen, internal segment of the globus pallidus, caudate nucleus, SN, and periaqueductal gray matter. *DRG*: dorsal root ganglia, *Olf*: olfactory bulb, *SG*: sympathetic ganglia. Semi-quantitative scale for LBs and NFTs: *dot-pattern* = 1–10, *gray* = 10–20, *black* > 20. Number of lesions in a field observed using a 10× objective. Iron-positive granules: *dot-pattern* = mild, *gray* = moderate, *black* = severe.